Contract No.:

This manuscript has been authored by Savannah River Nuclear Solutions (SRNS), LLC under Contract No. DE-AC09-08SR22470 with the U.S. Department of Energy (DOE) Office of Environmental Management (EM).

Manuscript Details

Manuscript number	JENVRAD_2016_58
Title	Characterizing the Detectability of Emission Signals from a North Korean Nuclear Detonation
Article type	Short Communication

Abstract

The detectability of emission sources, defined by a low-level of mixing with other sources, was estimated for various locations surrounding the Sea of Japan, including a site within North Korea. A high-resolution meteorological model coupled to a dispersion model was used to simulate plume dynamics for four periods, and two metrics of airborne plume mixing were calculated for each source. While emissions from several known sources in this area tended to blend with others while dispersing downwind, the North Korean plume often remained relatively distinct, thereby making it potentially easier to unambiguously ‘backtrack’ it to its source.

Keywords	Transport; Modeling; Detectability; Emissions
Taxonomy	3d Modeling, Radioactivity Release, Dispersion

Corresponding Author	David Werth
Corresponding Author's Institution	Savannah River National Laboratory
Order of Authors	David Werth, Robert Buckley
Suggested reviewers	Gerhard Wotawa, Paul Eslinger, Anders Ringbom

Submission Files Included in this PDF

File Name [File Type]

ArticleText.docx [Manuscript (without Author Details)]

Fig1.pdf [Figure]

Fig2.pdf [Figure]

Fig3.pdf [Figure]

Fig4.pdf [Figure]

Highlights.docx [Highlights]

ArticleCaptions.docx [Supporting File]

TitlePage.docx [Title Page (with Author Details)]

To view all the submission files, including those not included in the PDF, click on the manuscript title on your EVISE Homepage, then click 'Download zip file'.

1 1. Introduction

2 The Comprehensive Test Ban Treaty Organization (CTBTO) is charged with the
3 detection of clandestine nuclear detonations worldwide (Auer and Prior, 2014). This is to be
4 accomplished with an International Monitoring System (IMS) through 1) the detection of sonic
5 and seismic waves emitted from an explosion and 2) the monitoring of radionuclides expected to
6 be released (Wotawa et al., 2003; Auer and Prior, 2014), xenon in particular (Medalia, 2010;
7 Kokaji and Shinohara, 2014). This noble gas (created in nuclear explosions and as a decay
8 product of iodine, another fission product (Medalia, 2010)) is very difficult to contain
9 (Hafemeister, 2007; Wotawa et al., 2010), is detectable at low levels (Medalia, 2010) and can
10 form a signature for a nuclear test designed to elude the other sensors (Wotawa et al., 2003;
11 Kokaji and Shinohara, 2014). The half-lives of the xenon isotopes range from 9 hours to 12
12 days (Wotawa et al., 2010), allowing for detectable concentrations at long distances weeks after a
13 release (Medalia, 2010). As an example, early suggestions that emissions from the North
14 Korean test of February 2013 had been completely contained (Dahl, 2013) were refuted with the
15 April detections of a corresponding xenon signal by the IMS stations at Ussuriysk, Russia and
16 Takasaki, Japan (Ringbom et al., 2014). Similarly, the 2006 North Korean test emitted
17 radionuclides that were detected as far away as Canada (Saey, 2007; Kokaji and Shinohara,
18 2014).

19 It is desired that any signal detected at a sensor be ascribed to a known source, or else
20 flagged as being from an unknown source. To accomplish this, the Provisional Technical
21 Secretariat (PTS) of the CTBTO currently runs the FLEXPART diffusion model (Stohl et al.,
22 2005), forced with ECMWF 1^0 x 1^0 meteorological data (Wotawa et al., 2010) as part of its
23 Atmospheric Transport Model (ATM) system. This is used to calculate the 'source receptor
24 sensitivity' (SRS) – a matrix that relates the signal at any sensor location to all potential source
25 points (Wotawa et al., 2003). Given a detection at a subset of the sensors, the SRS can be used
26 to produce a 'Field of Regard' (FOR) – the area that influences all those sensors (and not others)

and could be the source region (Wotawa et al., 2003), as was done for the 2013 test (Ringbom et al., 2014). Atmospheric transport models coupled with meteorological models are powerful tools for recreating the motion of a plume from its point of emission to its detection at sensors (Kim et al., 2008; Eslinger et al., 2014; Arnold et al. 2015; Saito et al., 2015).

The ability to detect any signal and 'backtrack' it to its source depends on the proximity of that source to other sources, as transport modeling will associate the detected signal from a well dispersed plume to a large FOR that encompasses an overall potential source area of the plume, not just that of the clandestine signal. This could allow the emissions from a nuclear test to remain disguised as being from known sources. Radioxenon is released from nuclear power plants and medical isotope facilities (Kalinowski and Tuma, 2009; Matthews et al., 2010) as well as from a nuclear detonation, so the detection of a North Korean radioactive source is complicated by the existence of nuclear facilities in South Korea, China, and Japan (Wotawa et al., 2010). In particular, ^{133}Xe is emitted from weapons tests, reactor operations, and medical isotope facilities (Kokaji and Shinohara, 2014), and has a half-life of 5 days. While isotope ratios for nuclear detonations are different from other sources (Matthews et al., 2010), underground nuclear tests can mask this signature (Eslinger et al., 2014). Using isotope ratios to distinguish a clandestine test also requires the detection of ^{135}Xe (Kalinowski et al., 2008), which has a 9.14 hour half-life and may not be detectable if the gas is contained underground and leaks out weeks after the initial explosion.

Simulations of specific releases (e.g., the 2006 and 2013 NK tests) have demonstrated the ability to identify the source regions from signal detections combined with mesoscale modeling (Kim et al., 2008; Ringbom et al., 2009, 2014), and the simulation of a series of hypothetical releases has been used by Eslinger et al (2015) to derive general properties of radioactive plume dispersion. Similar to the latter, this research quantifies the ability to discriminate a clandestine North Korean (NK) signal from known signals for a series of hypothetical releases, using two defined metrics: the signal strength and the area overlap ratio of the plumes. Plume simulations

were done with a mesoscale meteorological model coupled to a transport model. By simulating emissions from locations surrounding the Sea of Japan for several periods, the degree to which the NK signal stands out from the known signals emitted in the same region was calculated and compared to the 'detectability' of the other sources in the region. It is demonstrated that an NK signal much greater than that of the surrounding sources is not required for detection, as such a clandestine signal is often distinct from the surrounding, known signals at some time during its existence.

2. Material and Methods

2.1 Modeling

The meteorological conditions were generated using the Regional Atmospheric Modeling System (RAMS) (Pielke et al., 1992). RAMS has been applied extensively to produce meteorological simulations on a range of scales (e.g. Cotton et al., 2003), and is ideal for this research. A domain over the Sea of Japan was selected, encompassing Japan and the Korean peninsula (Fig. 1). The model used two grids – a larger, outer grid at 30 km grid spacing, and an inner grid at 10 km spacing (Fig. 1a). The inner grid (depicted in Fig. 1b) comprises 251 × 251 grid points and was centered at 39°N, 133.5°E. The vertical spacing started at 30 m for the lowest level, and increased 15% for each successive level until a maximum vertical spacing of 500 m was reached. The model was run with the Harrington radiation scheme (Harrington, 1997), and the LEAF-2 land surface scheme (Walko et al., 2000). The Mellor-Yamada planetary boundary layer scheme (Mellor and Yamada, 1982) was used to calculate vertical turbulent (sub-grid scale) diffusion, with a Smagorinsky (1963) horizontal deformation scheme used for the horizontal diffusion. The model also used a 30 second (roughly 800 m) topographic field (Fig. 1b), which can resolve many of the interactions between orography and airflow. Boundary conditions were supplied using the Global Forecast System (GFS, Environmental Modeling Center 2003) output, with 0.5° horizontal resolution and at 3-hr intervals.

79 The detectability of a North Korean source can be sensitive to seasonal shifts in wind
80 patterns (Achim et al., 2013). Therefore, RAMS was run for four periods: Autumn (October 21st
81 through October 31st, 2012), Summer (July 22nd through July 28th, 2012), Winter (Feb 10th
82 through Feb 19th, 2013) and Spring (April 4th through April 15th, 2013). Data was saved every
83 10 minutes, allowing the dispersion simulations to resolve features with short time scales. The
84 RAMS meteorological output was subsequently used as input to the Hybrid Single-Particle
85 Lagrangian Integrated Trajectory dispersion model (HYSPLIT, Draxler and Hess, 1998).
86 HYSPLIT has been used in numerous applications (e.g., Becker et al., 2007; Butler et al., 2005;
87 Yerramilli et al., 2012; Stunder et al., 2007) related to simulating the large-scale dispersion of
88 emitted tracer. This Lagrangian model simulates the release of a large number of 'particles',
89 recalculating at each time step the position of each one according to both a resolved wind field
90 (from the RAMS model) and a dispersive term derived from the RAMS-simulated turbulence
91 kinetic energy. The particles begin at the release point as a concentrated cloud, which then
92 spread out and are transported downwind as the simulation progresses. Data from the first two
93 days of each coupled simulation (e.g., April 4th and 5th) were eliminated as spin-up.
94 The RAMS/HYSPLIT coupled models were run for the four periods with sources at eight
95 known source locations: nuclear power plants at Ohi, Wolsong, Hanbit, Hanul, Kori, Tianwan
96 and Qinshan, and a medical isotope production (MIP) facility (Fig. 1b). Ohi and MIP are in
97 Japan, Tianwan and Qinshan are in China, and the others are in South Korea. The two Chinese
98 sources are actually located slightly beyond the western edge of Grid 2, but were shifted eastward
99 (200 km for Tianwan, 60 km for Qinshan) for the simulation to allow them to serve as emission
100 sources. Although Ohi is currently not operational (Matsuyama, 2013), it was active during the
101 four selected periods (BBC, 2012). In addition, a hypothetical ninth source was located in
102 Punggye, North Korea (NK, indicated by the red star in Fig. 1), the site of previous underground
103 nuclear tests. Note also the locations of fixed CTBTO surface samplers in Japan at Takasaki
104 and in Russia at Ussuriysk, to be discussed later. An underground detonation will produce its

105 signature nuclides within a short time, but their release into the free atmosphere can be more
106 gradual - the signal detected in April from the February 2013 detonation was ascribed to a release
107 from a only few days earlier (Ringbom et al., 2014), indicating that the test site was either still
108 'leaking' xenon weeks after the detonation, or that surface conditions were altered near the test
109 site to allow for emissions out of the ground. It is therefore assumed in this work that all sources
110 are continuously emitting xenon at a rate of 1.37×10^4 GBq/yr, equivalent to the release rate at
111 the Hanul plant (Kalinowski and Tuma, 2009), and that it is not subject to atmospheric depletion.
112 We will not apply a factor for radioactive decay in the initial simulations, but will do so for
113 subsequent runs as described below. In the simulations conducted here, the plumes started as a
114 point source and tended to reach their maximum size after roughly 3 to 4 days, after which the
115 plume often exited the domain preventing further growth. Therefore, each detection can be
116 considered to be the result of a 3 to 4 day release. This is longer than has been observed
117 (Ringbom et al. (2014) estimated a 1.5-day release time for the April 2014 detection), but it
118 allows for the characterization of multiple releases/detections over an extended period.
119 The simulations calculated the instantaneous concentrations at all points within the
120 domain. In reality, however, sampler data represents tracer gas collected over a 12 to 24 hour
121 period, depending on the location (Kokaji and Shinohara, 2014; Wotawa et al., 2010), so a value
122 generated at a detector will actually represent a time-averaged value. This can cause two
123 separate plumes that arrive at the same location at different times to appear as one, making it
124 harder to discriminate between them. To account for this, the simulated concentration data was
125 subjected to a 12-hour averaging. Sensors also have a minimum concentration below which
126 they cannot detect a signal, and the currently described minimum detectability limit for CTBT
127 sensors is 0.1 mBq/m^3 (Wotawa et al., 2010), which we assumed here as well by setting all
128 simulated concentrations below this threshold to zero for purposes of characterizing signal
129 detectability.
130

131

132 2.2 Detectability

133 With the coupled simulations, the concentrations at each point for all sources can be
134 calculated, and the source interactions can be determined. Two measures of signal detectability
135 were applied. One measure of how strongly a signal stands out in a time series at a single point
136 is the 'signal strength' (*SS*) relative to the background, defined as:

137 $$\frac{q_{unk} - q_{kwn}}{q_{unk}},\ q_{unk} > q_{kwn}, \quad (1a)$$

138 $$SS = \begin{cases} \\ \end{cases}$$ $$0,\ q_{unk} < q_{kwn}, \quad (1b)$$

139 $$0,\ q_{unk} < q_{kwn}^{max}/20. \quad (1c)$$

140 The symbols q_{unk} and q_{kwn} represent the concentrations of the 'unknown' and 'known'
141 (i.e., produced by known sources) plumes at a point in the domain, respectively. The value of
142 q_{kwn}^{max} represents the maximum value of q_{kwn} in the time series, and Eq. 1c is implemented to
143 prevent very small signals from contributing to the *SS* metric. The *SS* at any detector ranges
144 from 0 (the unknown plume does not stand out amidst the known plumes or is weak relative to
145 the rest of the time series) to 1 (only the unknown plume is over the detector at that time).

146 The degree to which two airborne plumes are mixed (and difficult to discriminate) can
147 also be quantified by their area overlap ratio. The concept was applied by Pawson and Nielsen
148 (2010, hereafter referred to as PN10) to help relate measured global CO_2 concentrations to
149 potential sources. It can also be applied on a regional scale, and is similar to the 'figure of merit
150 in space' used by Straume (2001) to quantify the spatial overlap with observations of a simulated
151 plume. Define two plumes (*m* and *n*), each from a different source, of areas A_m and A_n.
152 Assume that plume *m* is from an unknown source, while plume *n* is from a known source, and the
153 two plumes have an overlap area $A_{m,n}$. The latter is defined as an area within which 1) both the
154 known and unknown sources exist, and 2) the value of *SS* is less than 0.9. The latter will allow
155 any location in which the unknown plume signal is over 10 times the known plume to be

156 considered as containing only the unknown plume. Our ability to ascribe a signal detection to
157 plume *m* and unambiguously rule out plume *n* as the true source is reduced by the fraction of
158 plume m that is 'contaminated' by plume *n*. PN10 quantified this fraction as

159 $$R_{m,n} = \frac{A_{m,n}}{A_m} \quad (2)$$

160 $R_{m,n} = 1$ implies a complete overlap of signals, whereas when $R_{m,n} = 0$ there is perfect
161 detectability (i.e., no overlap). Ideally, values of $R_{m,n}$ will be low for the North Korean source,
162 indicating that the clandestine plume is not well mixed with the known sources, making it
163 theoretically easier to rule out the latter as the source of any detection.

164 The *SS* and $R_{m,n}$ can be calculated for various known and unknown source combinations -
165 each of the actual sources can in turn be assigned as the 'unknown' source, with all of the
166 remaining sources serving as the 'known' sources, allowing for an estimate of the separation
167 necessary for the detection of a signal. Figure 1b shows that some sources are more remote than
168 others, and the variation in detectability for Wolsong, Ohi, and NK was determined.

169

170 3. Results and Discussion

171 The Korean nuclear plant at Wolsong is located within very close proximity to several
172 other sources on the Korean peninsula (Fig. 1b), and it is therefore expected to be difficult to
173 discern that source from the others. Maps for the February and October simulations show how
174 this 'unknown' plume was mostly hidden within the combined plumes of the other stations,
175 failing to stand out above the known sources (Fig. 2, left), and values of $R_{m,n}$ are high for this
176 source, usually greater than 0.9 for all seasons (Fig. 3).

177 The Japanese power station at Ohi (Fig. 2, middle) is more remote from the other sources,
178 and its signal is expected to remain distinct from the others. Periods of good detectability - Feb.
179 14th at 1200 UTC (Fig. 3a) and Oct. 25th at 1200 UTC (Fig. 3d) - alternated with periods when the
180 plumes are too mixed to be considered detectable (Feb. 16th at 0000 UTC (Fig. 3a)). The values

181 of $R_{m,n}$ were lower than for Wolsong as the unknown source is now more distant from the known
182 sources, though detectability was greater for February and October (Fig. 2, Fig. 3), with more
183 mixing in April and July (Figs. 3b,c).

184 For the NK release, we assumed the combined plumes from the eight actual known
185 sources represent the 'known' plume, while the hypothetical NK plume represented a ninth
186 'unknown' plume. For February and October, periods of weak mixing (e.g., Feb. 14th at 0000
187 UTC and Oct. 25th at 0000 UTC) (Fig. 2, right; Fig. 3a, d) alternated with periods when the plume
188 was well mixed (Feb. 19th at 0000 UTC (Fig. 3a) and Oct. 29th at 0000 UTC (Fig. 3d)), similar to
189 Ohi. Overall detectability was greatest for April, with stronger plume mixing in July.

190 The above results are mostly a function of wind direction. The NK source lies further
191 north than the others, so westerly or northwesterly winds will tend to allow for a large plume to
192 extend from that source without interacting with other known sources. The winds for the latter
193 half of the April simulation are mostly from the west, allowing for periods of low $R_{m,n}$ (Fig. 3b).
194 The February and October simulations were also characterized by periods of northwest and
195 westerly winds, allowing for periods in which approximately 1/3rd of the NK plume was distinct
196 from the known tracer (Fig. 3a, d). The July simulation, however, was dominated by
197 southwesterly winds, which allowed the South Korean and Chinese sources to mix with the NK
198 plume and reduce its detectability (only about 10% of the plume is unmixed) (Fig. 3c).

199 A dispersion model can aid in unknown source detection by identifying the existing
200 sensor locations most likely to detect a signal from a suspected source (the 'catch the plume
201 scenario' as outlined by Ross (2010)), or in identifying promising locations for the deployment of
202 a mobile detector (as was done after the 2016 North Korean nuclear test (Lamothe, 2016)).
203 Figure 2 (right) indicates that 'pure' tracer from NK passed over central Japan around October
204 25th and southeastern Russia on Feb. 14th, with tracer from NK over other parts of the domain
205 thoroughly mixed with tracer from the other sources. The simulated time series of tracer at the
206 CTBT sensor location at Ussuriysk (the yellow circle in Fig. 1b) shows a detectable NK signal for

each of the 4 simulations (Fig. 4), existing either as a pure signal or as the dominant component of a mixed signal (with a large signal strength). The tracer concentrations at Takasaki (not shown) also indicate tracer for the April and October simulations. Also note that Ussuriysk detected a strong signal in July (Fig. 4c), despite the fact that strong plume mixing occurred during this simulated period (Fig. 3c).

Given that ^{133}Xe (half-life of 5 days) is the only isotope of xenon released from a weapons test, a nuclear reactor, and a medical isotope facility (Kokaji and Shinohara, 2014), we reran the February analysis accounting for radioactive decay. This implied a weaker weapons test signal among the other possible sources. Due to the relatively short transport time, the *SS* patterns in Fig. 2a and the values of R seen in Fig. 3a are little altered when the 5-day decay was imposed (not shown), and the time series in Fig. 4a are only reduced by 10-20%, with the signal from the North Korean test still clear in the data.

4. Conclusions

Simulations of releases in the area surrounding the Sea of Japan with a high-resolution mesoscale transport model indicated that, despite the existence of other sources in the region, the source in Punggye, North Korea is discernable for much of the time during three of the four periods, each representing a different season, considered here. During these times, the FOR of the two nearby CTBT detectors will tend to encompass NK, while excluding other potential source regions. This supports the established use of transport modeling and the application of the FOR to reveal nuclear detonations within NK, and indicates that a North Korean signal need not be significantly higher than the confounding nearby sources to be detected. Even with substantial mixing, a well-placed detector will often be within the area of the 'clean' signal (e.g., the July simulation).

Application of this technique in the wake of an actual suspected weapon test requires a more thorough knowledge of source variability and strength in time. The application shown here

assumed all sources were continuously emitting radioactivity into the atmosphere at the same release rate for all sources. Facilities that emit radionuclides often operate intermittently (Wotawa et al., 2010), and variability in source strength will necessarily alter the conclusions reached in the examples shown here. Given the wind patterns, it is likely that xenon from the February 2013 NK test remained sequestered until shortly before its release and detection two months later (Ringbom et al., 2014).

A nuclear detonation will produce radionuclides ~7 orders of magnitude greater than the daily output of a nuclear plant (Matthews et al., 2010). An underground test will likely experience a reduced rate of release, however, with the result often being a signal only modestly stronger than the regional background (e.g., Ringbom et al., 2014; Eslinger et al., 2015). For the foreseeable future, the detection of airborne nuclides from a North Korean nuclear test will be confounded by the presence of other facilities near the Sea of Japan with a similar signature. High resolution mesoscale modeling will therefore remain a crucial component of the global monitoring system.

Acknowledgments

The authors gratefully acknowledge the NOAA Air Resources Laboratory (ARL) for the provision of the HYSPLIT transport and dispersion model and/or READY website (http://www.ready.noaa.gov) used in this publication.

Funding for this study was provided by the U.S. Department of Energy and the Laboratory Directed Research and Development Program at the Savannah River National Laboratory. SRNL is operated by Savannah River Nuclear Solutions for the U.S. Department of Energy under contract number DE-AC09-08SR22470.

References

Achim, P., Morin, M., Gross, P., Le Petit, G., Monfort, M., 2013. Highlighting radioxenon local sources by studying the seasonal variability of worldwide atmospheric background. Application to JPX38-Takasaki detections. CTBTO Science and Technology Conference, http://www.ctbto.org/fileadmin/snt2013/posters/T1-P30.pdf. Last accessed August 16th, 2016.

Arnold, D., Maurer, C., Wotawa, G., Draxler, R., Saito, K., Seibert, P., 2015. Influence of the meteorological input on the atmospheric transport modelling with FLEXPART of radionuclides from the Fukushima Daiichi nuclear accident. *Journal of Environmental Radioactivity,* **139**, 212-225.

Auer, M., Prior, M., 2014. A New Era of Nuclear Test Verification. *Physics Today*, Sept. 2014.

BBC, 2012. Japan switches on Ohi nuclear reactor amid protests, http://www.bbc.com/news/world-asia-18662892. Last accessed August 16th, 2016.

Becker, A., Wotawa, G., De Geer, L.-E., Seibert, P., Draxler, R.R., Sloan, C., D'Amours, R., Hort, M., Glaab, H., Heinrich, P., Grillon, Y., Shershakov, V., Katayama, K., Zhang, Y., Stewart, P., Hirtl, M., Jean, M., Chen, P., 2007. Global backtracking of anthropogenic radionuclides by means of a receptor oriented ensemble dispersion modelling system in support of Nuclear-Test-Ban Treaty verification. *Atmospheric Environment*, **41**, 4520-4534.

Butler, T.J., Likens, G., Vermeylen, F., Stunder, B., 2005. The impact of changing nitrogen oxide emissions on wet and dry nitrogen deposition in the northeastern USA. *Atmospheric Environment,* **39**, 4851-4862.

Cotton,W. , Pielke, R.,Walko, R., Liston, G., Tremback, C., Jiang, H., McAnelly, R., Harrington, J., Nicholls, M., Carrio, G., McFadden, J., 2003. RAMS 2001: Current status and future directions. *Meteorol. Atmos. Phys*., **82**, 5–29.

Dahl F., 2013. No "smoking gun" from North Korean nuclear test. Reuters, http://www.reuters.com/article/2013/03/12/us-nuclear-northkorea-test-ban-idUSBRE92B0J220130312. Last accessed August 16th, 2016.

Draxler, R.R., Hess G. D., 1998. An overview of the HYSPLIT_4 Modelling System of Trajectories, Dispersion, and Deposition. *Aust. Meteor. Mag*., **47**, 295-308.

Environmental Modeling Center, 2003. The GFS Atmospheric Model. NOAA/NCEP/Environmental Modeling Center Office Note 442, 14 pp. [Available online at http://www.emc.ncep.noaa.gov/officenotes/FullTOC.html.]

Eslinger, P., Biegalski, S., Bowyer, T., Cooper, M., Haas, D., Hayes, J., Hoffman, I., Korpach, E., Yi, J., Miley, H., Rishel, J., Ungar, K., White, B., Woods, V. 2014. Source term estimation of radioxenon released from the Fukushima Dai-ichi nuclear reactors using measured air concentrations and atmospheric transport modeling. *Journal of Environmental Radioactivity,* **127**, 127-132.

Eslinger P., Bowyer, T., Cameron, I., Hayes, J., Miley, H., 2015. Atmospheric plume progression as a function of time and distance from the release point for radioactive isotopes. *Journal of Environmental Radioactivity*, **148,** 123-129.

Hafemeister, D., 2007. Progress in CTBT Monitoring Since its 1999 Senate Defeat. *Science and Global Security*, **15**, 151-183.

Harrington, J., 1997. The effects of radiative and microphysical processes on simulated warm and transition season Arctic stratus. Department of Atmospheric Science Bluebook 637, Colorado State University, Fort Collins, CO, 289 pp.

Kalinowski, M., Becker, A., Saey, P., Tuma, M., Wotawa, G., 2008. The Complexity of CTBT Verification. Taking Noble Gas Monitoring as an Example. *Complexity*, **14**, 89-99.

Kalinowski, M., Tuma, M., 2009. Global radioxenon emission inventory based on nuclear power reactor reports. *Journal of Environmental Radioactivity*, **100**, 58-70.

Kim, C.H., Song, C.K., Lee, S.H., Song, S.K., 2008. Simulating mesoscale transport and diffusion of radioactive noble gases using the Lagrangian particle dispersion model. *Journal of Environmental Radioactivity,* **99***,* 1644-1652.

Kokaji, L., Shinohara, N., 2014. Radiochemical Verification Technologies for the Detection of Nuclear Explosions – Recent Developments in Radionuclide Monitoring with the Comprehensive Nuclear-Test-Ban Treaty. *Jour. Nucl. and Radiochem. Sci*., **14**, 1-9.

Lamothe, D., 2016. This is the Air Force radiation sniffer deploying after North Korea's nuclear test. January 6th, The Washington Post, https://www.washingtonpost.com/news/checkpoint/wp/2016/01/06/this-is-the-air-force-radiation-sniffing-plane-deploying-after-north-koreas-nuclear-test/. Last accessed August 16th, 2016.

Matsuyama, K., 2013: Shutdown of Japan's Last Nuclear Reactor Raises Power Concerns, Bloomberg, http://www.bloomberg.com/news/articles/2013-09-16/shutdown-of-japan-s-last-nuclear-reactor-raises-power-concerns. Last accessed August 16th, 2016.

Matthews, M. and co-authors, 2010. Workshop on Signatures of Medical and Industrial isotope production – A Review. Pacific Northwest National Laboratory, PNNL-19294

Medalia, J., 2010. North Korea's 2009 Nuclear Test: Containment, Monitoring, Implications. Congressional Research Service, 7-5700, R41160, www.crs.gov

Mellor, G. L., Yamada, T., 1982. Development of a turbulence closure model for geophysical fluid problems. *Rev. Geophys. Space Phys*., **20**, 851–875.

Pawson, S. Nielsen, J., 2010. Using High-Resolution Forward Model Simulations of Ideal Atmospheric Tracers to Assess the Spatial Information Content of Inverse CO_2 Flux Estimates. AGU 2010 Fall Meeting – San Francisco, CA – Session A54D – December 17, 2010

Pielke, R. A., Cotton, W. R., Walko, R. L., Tremback, C. J., Lyons, W. A., Grasso, L. D., Nicholls, M. E., Moran, M. D., Wesley, D. A., Lee, T. J., Copeland, J. H., 1992. A Comprehensive Meteorological Modeling System – RAMS. *Meteorol. Atmos. Phys*., **49**, 69–91.

Ringbom, A., Elmgreen, K., Lindh, K., Peterson, J., Bowyer, T., Hayes, J., McIntyre, J., Panisko, M., Williams, R., 2009. Measurements of radioxenon in ground level air in South Korea following the claimed nuclear test in North Korea on October 9, 2006. *J. Radioanal. Nucl. Chem*., **282**, 773-779.

Ringbom A., Axelsson A., Aldener M., Auer M., Bowyer T.W., Fritioff T., Hoffman I., Khrustalev K., Nikkinen M., Popov V., Popov Y., Ungar K., Wotawa G. 2014. Radioxenon detections in the CTBT international monitoring system likely related to the announced nuclear test in North Korea on February 12, 2013. *Journal of Environmental Radioactivity*, **128**, 47-63.

Ross, J., 2010. Simulation of atmospheric krypton-85 transport to assess the detectability of clandestine nuclear reprocessing. Reports on Earth System Science, Phd. D. Dissertation, University of Hamburg, http://www.mpimet.mpg.de/fileadmin/publikationen/Reports/WEB_BzE_82.pdf**.** Last accessed August 16th, 2016.

Saey, P. R. J., Bean, M., Becker, A., Coyne, J., d'Amours, R., De Geer, L.-E., Hogue, R., Stocki, T. J., Ungar, R. K., Wotawa, G., 2007. A long distance measurement of radioxenon in Yellowknife, Canada, in late October 2006. *Geophys. Res. Lett*., **34**, *L20802, doi:*10.1029/2007GL030611.

Saito, K., Shimbori, T., Draxler, R., 2015. JMA's regional atmospheric transport model calculations for the WMO technical task team on meteorological analyses for Fukushima Daiichi Nuclear Power Plant accident. *Journal of Environmental Radioactivity*, **139**, 185-199.

Smagorinsky, J., 1963. General circulation experiments with the primitive equations. Part I, The basic experiment. *Mon. Wea. Rev*., **91**, 99-164.

357 Stohl, A., Forster, C., Frank, A., Seibert, P., Wotawa, G., 2005. Technical note: The
358 Lagrangian particle dispersion model FLEXPART version 6.2. *Atmos. Chem. Phys*., **5**, 2461-
359 2474.
360 Straume, A. 2001. A More Extensive Investigation of the Use of Ensemble Forecasts for
361 Dispersion Model Evaluation. *J. Appl. Meteor.*, **40**, 425–445.
362 Stunder, B., Heffter, J., Draxler, R., 2007. Airborne Volcanic Ash Forecast Area
363 Reliability. *Wea. Forecasting*, **22**, 1132–1139.
364 Walko, R., Band, L., Baron, J., Kittel, T., Lammers, R., Lee, T., Ojima, D., Pielke Sr., R.,
365 Taylor, C., Tague, C., Tremback, C., Vidale, P., 2000. Coupled Atmosphere–Biophysics–
366 Hydrology Models for Environmental Modeling. *J. Appl. Meteor.*, **39**, 931–944.
367 Wotawa, G., De Geer L., Denier P., Kalinowski M., Toivonen H., D'Amours R., Desiato
368 F., Issartel J.-P., Langer M., Seibert P., Frank A., Sloan C., Yamazawa H., 2003. Atmospheric
369 transport modelling in support of CTBT verification—overview and basic concepts. *Atm. Env*.,
370 **37**, 2529-2537.
371 Wotawa G., Becker, A., Kalinowski, M., Saey, P., Tuma, M., Zähringer, M., 2010.
372 Computation and Analysis of the Global Distribution of the Radioxenon Isotope ^{133}Xe based on
373 Emissions from Nuclear Power Plants and Radioisotope Production Facilities and its Relevance
374 for the Verification of the Nuclear-Test-Ban Treaty. *Pure Appl. Geophys*., **167**, 541-557.
375 Yerramilli, A., and co-authors, 2012. An integrated WRF/HYSPLIT modeling
376 approach for the assessment of PM2.5 source regions over the Mississippi Gulf Coast region. *Air*
377 *Qual. Atmos. Health*, **5**, 401-412.
378

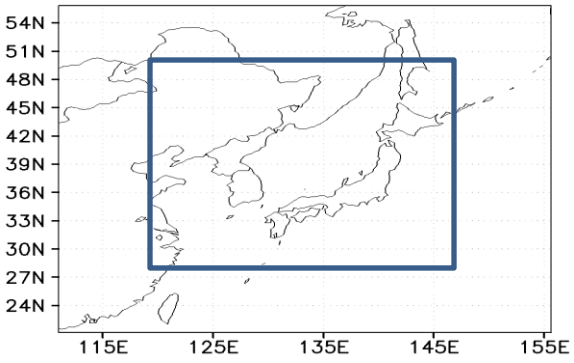
54N
51N
48N
45N
42N
39N
36N
33N
30N
27N
24N
115E
125E
135E
145E
155E

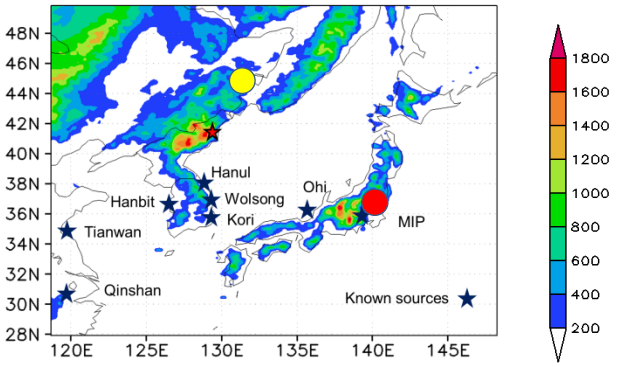
48N
46N
44N
42N
40N
38N
36N
34N
32N
30N
28N
120E
125E
130E
135E
140E
145E
Hanul
Hanbit
Wolsong
Kori
Ohi
MIP
Tianwan
Qinshan
Known sources
1800
1600
1400
1200
1000
800
600
400
200

a)

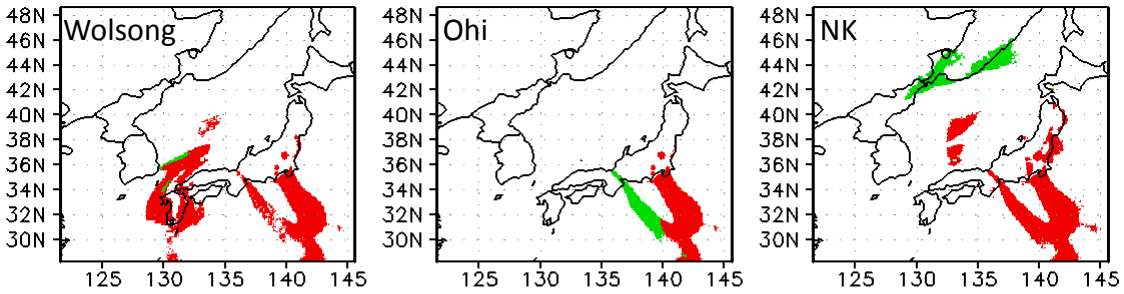
Wolsong
Ohi
NK
48N
46N
44N
42N
40N
38N
36N
34N
32N
30N
125
130
135
140
145

b)

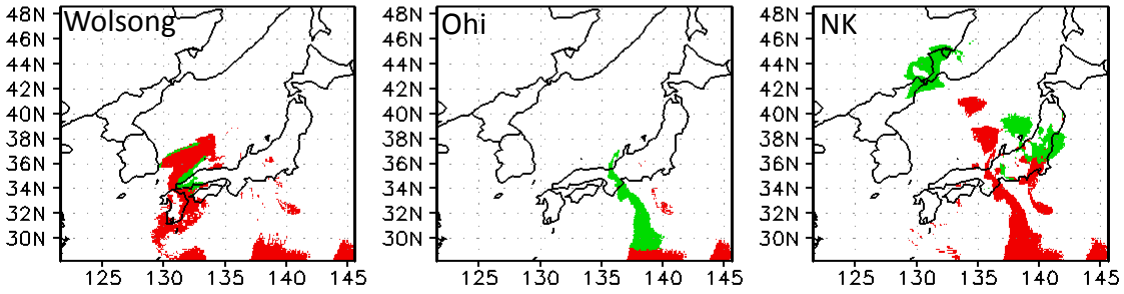
Wolsong
Ohi
NK
48N
46N
44N
42N
40N
38N
36N
34N
32N
30N
125
130
135
140
145

a)

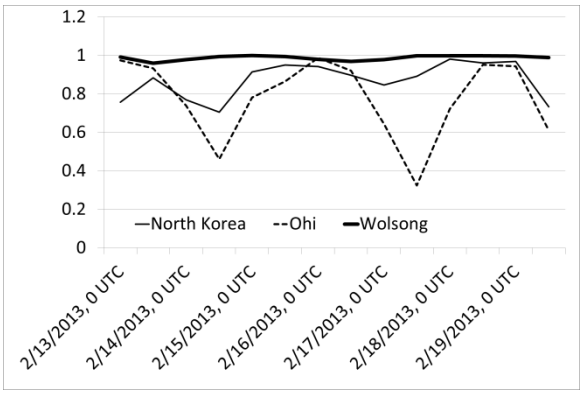
1.2
1
0.8
0.6
0.4
0.2
0
—North Korea
--Ohi
—Wolsong
2/13/2013, 0 UTC
2/14/2013, 0 UTC
2/15/2013, 0 UTC
2/16/2013, 0 UTC
2/17/2013, 0 UTC
2/18/2013, 0 UTC
2/19/2013, 0 UTC

b)

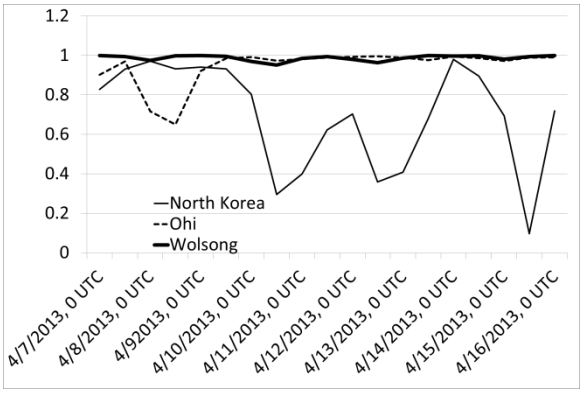
1.2
1
0.8
0.6
0.4
0.2
0
—North Korea
--Ohi
—Wolsong
4/7/2013, 0 UTC
4/8/2013, 0 UTC
4/92013, 0 UTC
4/10/2013, 0 UTC
4/11/2013, 0 UTC
4/12/2013, 0 UTC
4/13/2013, 0 UTC
4/14/2013, 0 UTC
4/15/2013, 0 UTC
4/16/2013, 0 UTC

c)

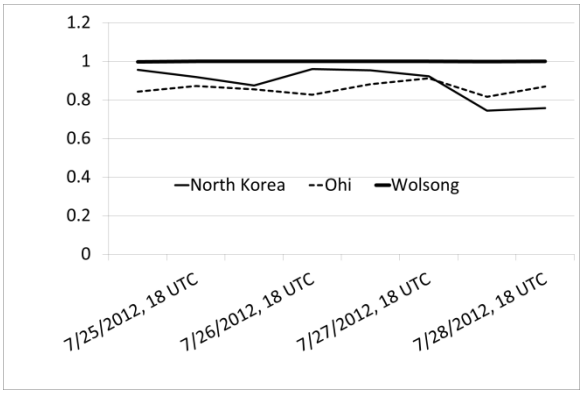
1.2
1
0.8
0.6
0.4
0.2
0
—North Korea
--Ohi
—Wolsong
7/25/2012, 18 UTC
7/26/2012, 18 UTC
7/27/2012, 18 UTC
7/28/2012, 18 UTC

d)

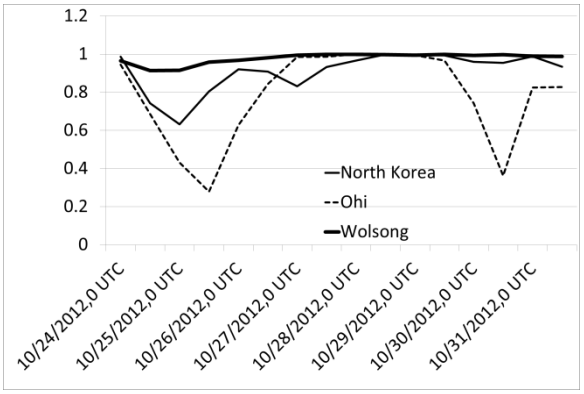
1.2
1
0.8
0.6
0.4
0.2
0
—North Korea
--Ohi
—Wolsong
10/24/2012,0 UTC
10/25/2012,0 UTC
10/26/2012,0 UTC
10/27/2012,0 UTC
10/28/2012,0 UTC
10/29/2012,0 UTC
10/30/2012,0 UTC
10/31/2012,0 UTC

a)

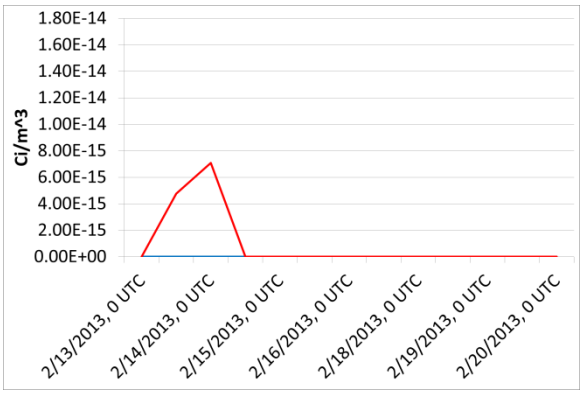
1.80E-14
1.60E-14
1.40E-14
1.20E-14
1.00E-14
8.00E-15
6.00E-15
4.00E-15
2.00E-15
0.00E+00
Ci/m^3
2/13/2013, 0 UTC
2/14/2013, 0 UTC
2/15/2013, 0 UTC
2/16/2013, 0 UTC
2/18/2013, 0 UTC
2/19/2013, 0 UTC
2/20/2013, 0 UTC

b)

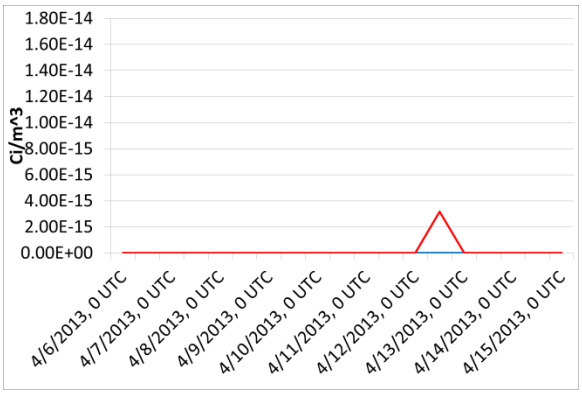
1.80E-14
1.60E-14
1.40E-14
1.20E-14
1.00E-14
8.00E-15
6.00E-15
4.00E-15
2.00E-15
0.00E+00
Ci/m^3
4/6/2013, 0 UTC
4/7/2013, 0 UTC
4/8/2013, 0 UTC
4/9/2013, 0 UTC
4/10/2013, 0 UTC
4/11/2013, 0 UTC
4/12/2013, 0 UTC
4/13/2013, 0 UTC
4/14/2013, 0 UTC
4/15/2013, 0 UTC

c)

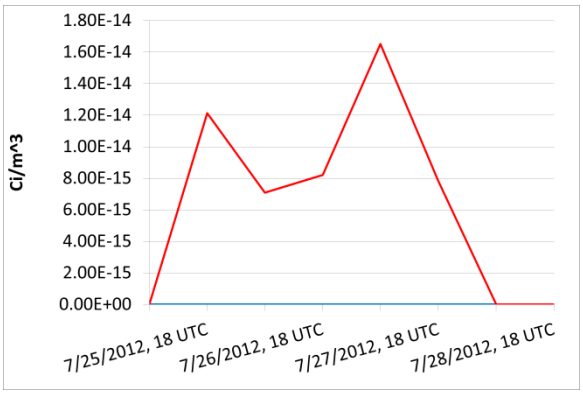
1.80E-14
1.60E-14
1.40E-14
1.20E-14
1.00E-14
8.00E-15
6.00E-15
4.00E-15
2.00E-15
0.00E+00
Ci/m^3
7/25/2012, 18 UTC
7/26/2012, 18 UTC
7/27/2012, 18 UTC
7/28/2012, 18 UTC

d)

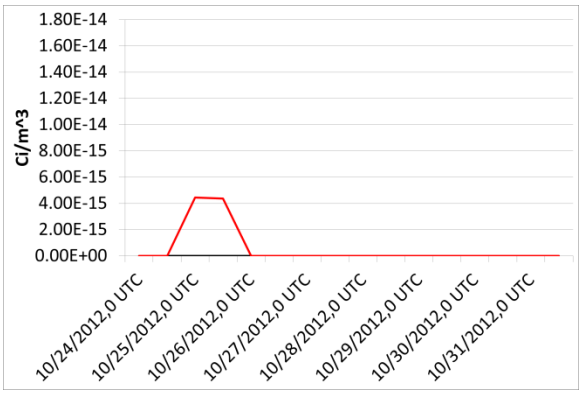
1.80E-14
1.60E-14
1.40E-14
1.20E-14
1.00E-14
8.00E-15
6.00E-15
4.00E-15
2.00E-15
0.00E+00
Ci/m^3
10/24/2012,0 UTC
10/25/2012,0 UTC
10/26/2012,0 UTC
10/27/2012,0 UTC
10/28/2012,0 UTC
10/29/2012,0 UTC
10/30/2012,0 UTC
10/31/2012,0 UTC

- Despite the existence of other sources in the region, the source in Punggye, North Korea is discernable for much of the time during three of the four periods, each representing a different season, considered here.

- This supports the established use of transport modeling and the application of the field of regard to reveal nuclear detonations within North Korea, and indicates that a North Korean signal need not be significantly higher than the confounding nearby sources to be detected.

- Even with substantial mixing, a well-placed detector will often be within the area of the ‘clean’ signal.

Figure 1 a) RAMS grids 1 and 2. b) Grid 2, with topography (m) shaded and sources (including the hypothetical source in North Korea) indicated by stars. The circles indicate the CTBTO monitoring stations at Takasaki (red) and Ussuriysk (yellow).

Figure 2 Area of the unknown plume over which the $SS > .9$ (green) and the $SS < .9$ (red) for the unknown source located at (left) Wolsong, (middle) Ohi, and (right) NK on February 14th, 0000 UTC (top), and October 25th, 0000 UTC (bottom). Note that locations where the unknown source is greater than zero but below the threshold are not colored, while area over which the combined known and unknown signals are above the threshold are colored, even if the individual signals are below the threshold.

Figure 3 Values of $R_{m,n}$ for the different 'unknown' sources for the a) February, b) April, c) July, and d) October simulations.

Figure 4 Tracer concentrations from NK (red) and all other sources (blue) at the Ussuriysk
CTBT detector (44.2 ºN, 132 ºE) for a) February, b) April, c) July, and d) October.

Characterizing the Detectability of Emission Signals from a North Korean Nuclear Detonation

David Werth[1]

Robert Buckley[1]

[1] Savannah River National Laboratory, Building 773-A, Aiken, SC 29808
Corresponding Author: David Werth, Savannah River National Laboratory, Building 773-A, Aiken, SC 29808, David.Werth@srnl.doe.gov, 803-725-3717, Fax No. 803-725-4233